FFI RAPPORT

THERMAL EFFECTS IN END-PUMPED SOLID STATE LASERS – Influence on resonator stability, beam quality, and output power

STENERSEN Knut, LIPPERT Espen, RUSTAD Gunnar, ARISHOLM Gunnar

FFI/RAPPORT-2001/03865

FFIE/792/115

Approved
Kjeller 30 July 2001

Stian Løvold
Director of Research

THERMAL EFFECTS IN END-PUMPED SOLID STATE LASERS - Influence on resonator stability, beam quality, and output power

STENERSEN Knut, LIPPERT Espen, RUSTAD Gunnar, ARISHOLM Gunnar

FFI/RAPPORT-2001/03865

FORSVARETS FORSKNINGSINSTITUTT
Norwegian Defence Research Establishment
P O Box 25, NO-2027 Kjeller, Norway

FORSVARETS FORSKNINGSINSTITUTT (FFI)
Norwegian Defence Research Establishment

P O BOX 25
N0-2027 KJELLER, NORWAY

UNCLASSIFIED

SECURITY CLASSIFICATION OF THIS PAGE
(when data entered)

REPORT DOCUMENTATION PAGE

1) PUBL/REPORT NUMBER	2) SECURITY CLASSIFICATION	3) NUMBER OF PAGES
FFI/RAPPORT-2001/03865	UNCLASSIFIED	33
1a) PROJECT REFERENCE	**2a) DECLASSIFICATION/DOWNGRADING SCHEDULE**	
FFIE/792/115	-	

4) TITLE

THERMAL EFFECTS IN END-PUMPED SOLID STATE LASERS - Influence on resonator stability, beam quality, and output power

5) NAMES OF AUTHOR(S) IN FULL (surname first)

STENERSEN Knut, LIPPERT Espen, RUSTAD Gunnar, ARISHOLM Gunnar

6) DISTRIBUTION STATEMENT

Approved for public release. Distribution unlimited. (Offentlig tilgjengelig)

7) INDEXING TERMS

IN ENGLISH:	IN NORWEGIAN:
a) solid lasers	a) faststofflasere
b) optical resonators	b) optiske resonatorer
c) thermal analysis	c) termisk analyse
d) stability criteria	d) stabilitetskriterier
e) birefringence	e) dobbeltbrytning

THESAURUS REFERENCE:

8) ABSTRACT

A theoretical analysis is given of the magnitudes of thermal effects in end-pumped high-power solid state lasers, and their influence on the laser output characteristics, particularly the beam quality and conversion efficiency. The theory of thermal lensing and stress-induced birefringence found in laser textbooks for the case of top-hat pump- and resonator modes, is extended to cover the more general case of Gaussian modes. Analytic expressions for these cases are derived. Expressions are also derived for the reduction of the birefringence loss, which can be achieved by inserting a quarter-wave plate between the laser rod and the laser end mirror. An analysis is given of the tolerance of laser resonators to thermal lensing, providing guide lines for the choice of resonator parameters in order to ensure sufficient resonator stability margins. Finally, a few examples are given of the results of rigorous numerical simulations of an end-pumped Nd:YAG laser. It is found that the analytic theory provides fairly good guide lines concerning the choice of resonator parameters in many cases, but there are also cases where the numerical simulations provide quite surprising results. In particular, it is found that good performance can be obtained even if the thermal focal length on the laser rod axis is substantially shorter than the limit for a stable resonator. For optimal choices of resonator parameters and pump beam diameter, it is found that a 50 W pump beam at 808 nm can be converted to more than 20 W output at 1064 nm, with a beam quality of $M^2 < 2$.

9) DATE	AUTHORIZED BY This page only	POSITION
30 July 2001	Stian Løvold	Director of Research

ISBN-82-464-0531-4

UNCLASSIFIED

SECURITY CLASSIFICATION OF THIS PAGE
(when data entered)

CONTENTS

THERMAL EFFECTS IN END-PUMPED SOLID STATE LASERS - Influence on resonator stability, beam quality, and output power

1 INTRODUCTION

The purpose of this report is to make an analysis of the influence of thermal effects on the performance characteristics of diode end-pumped solid state lasers, and particularly discuss the optimization of the laser resonator in the presence of such effects. The analysis is relevant for many types of end-pumped lasers, but is primarily focussed on near-infrared (1-2 μm) high power (10-50 W) lasers based on rare earth doped crystals, such as Nd:YAG, Tm:YAG, Ho:YAG, etc. Emphasis is put on aspects which are important for achieving high conversion efficiency and high beam quality. The motivation behind this work is the need for such sources as pump sources for optical parametric oscillators (OPOs) for generation of radiation in the mid-infrared atmospheric transmission windows (3-5 μm and 8-12 μm). These wavelength bands are used by a variety of military imaging sensors (thermal cameras and missile seekers), and there is an urgent military need for efficient laser sources in these bands, especially for countermeasure actions against such sensors.

The most important requirement for the solid state laser sources to be treated here is the ability to provide the required output power in a high-quality laser beam and with a high conversion efficiency. In order to achieve this, it is necessary to use a laser geometry where the diode pump light is efficiently coupled into and absorbed in the laser crystal, and the pumped crystal volume should have a small cross section and be well matched to the lowest order laser resonator mode. These conditions are usually best achieved in end-pumping geometries, as long as the beam quality of the pump diode is reasonably good and the pump absorption length is sufficiently small. As the output power of such diode pumped lasers is scaled to levels of 10s of watts, it is necessary to use large diode pump arrays (typically 1 cm long diode bars), which have very poor beam quality and are not directly suitable for end pumping of a laser rod. In a separate report [1] we have discussed a beam transformation technique, invented at the University of Southampton [2], which can be used to transform the output from such diode bars into a near cylindrical pump beam with a diameter of less than 0.5 mm over a propagation distance of a few mm (typical absorption length for the pump light in the laser crystal). The reader is referred to that report for the technical details of the beam transformation technique. Here we shall for simplicity make the assumption that the transformed pump beam can be approximated by a Gaussian beam over the relevant propagation distance in the laser crystal.

The most difficult challenge in the design of such high-power end-pumped lasers is the handling of thermal problems that arise due to the high heat load in the small crystal volume. Most notably, the heat load leads to large temperature gradients both in the radial and axial directions referred to the pump beam axis. Such gradients may lead to severe thermal lensing effects due to the temperature dependence of the refractive index, and to large local stresses which induce a spatially varying birefringence and depolarization and may, in the worst event, lead to crystal fracture. The effects of thermal lensing and birefringence, and methods for

compensation, are treated in Sections 2 and 3. The occurrence of thermal lensing may have serious implications on the stability conditions of the laser resonator, so it is necessary to take this into account in the resonator design. This is treated analytically in Section 4, whereas examples of complete laser simulations, taking the thermal lensing effects into account, are given in Section 5, using an advanced numerical simulation model.

The treatment is intended to be quite general, and more detailed treatments of special laser systems, including both simulations and experimental results, will be given in separate reports. The report provides analytic expressions which are useful for estimating the magnitude of thermal lensing and birefringence, and it provides guide lines concerning the laser resonator design in the presence of such effects.

2 THERMAL LENSING

2.1 Uniformly pumped laser rod

The problem of calculating the temperature distribution and thermally induced focal length has been treated in considerable detail in reference [3]. In the case of a cylindrical laser rod which is *uniformly heated* and *radially* cooled through the cylinder surface, analytic expressions are found for the radial temperature distribution and the thermally induced lens. In this case the radial temperature distribution becomes parabolic, and the focal length of the thermal lens can be approximated by:

$$f_{r,\phi} = \frac{1}{-2L\dfrac{\partial^2 T}{\partial r^2}\left\{\dfrac{1}{2}\dfrac{\partial n}{\partial T} + \alpha C_{r,\phi} n^3 + \dfrac{\alpha r_0 (n-1)}{L}\right\}} = \frac{1}{\dfrac{P_h}{k\pi r_0^{\,2}}\left\{\dfrac{1}{2}\dfrac{\partial n}{\partial T} + \alpha C_{r,\phi} n^3 + \dfrac{\alpha r_0 (n-1)}{L}\right\}} \qquad (2.1)$$

where

- $f_{r,\phi}$ - focal length of the thermal lens for the radial (r) and tangential (ϕ) polarization components of the laser field
- r_0 - rod radius
- L - rod length
- n - refractive index
- k - thermal conductivity
- α - thermal expansion coefficient
- $C_{r,\phi}$ - functions depending on the elastooptic coefficients in the rod material (influencing the refractive index of light polarized in the radial (r) and tangential (ϕ) direction, respectively, and leading to bi-focusing and birefringence)
- P_h - heat power (assumed to be *uniformly* distributed over the rod cross section)
- T - temperature
- r - radial distance from rod axis

In the most common host crystal, YAG, and near room temperature, we have [3]:

n = 1.82
k = 0.13 W/cm·K
α = $7.5 \cdot 10^{-6}$ /K
dn/dT = $7.3 \cdot 10^{-6}$ /K
C_r = 0.017
C_ϕ = -0.0025

The 3 terms in the curly brackets in the denominator in (2.1) account for the contributions to thermal lensing from the temperature dependence of the refractive index (first term), the stress dependence of the refractive index (second term), and the stress induced curvature of the rod ends (third term). The magnitudes of the 3 terms are approximately:

First term:	$(1/2)dn/dT$	$\approx 3.7 \cdot 10^{-6}$ /K
Second term (r):	$\alpha C_r n^3$	$\approx 0.77 \cdot 10^{-6}$ /K
Second term (ϕ):	$\alpha C_\phi n^3$	$\approx -0.11 \cdot 10^{-6}$ /K
Third term:	$\alpha r_0(n-1)/L$	$\approx (r_0/L) \cdot 6 \cdot 10^{-6}$ /K

We note that the second term contributes with up to 20 % of the first term, and that it will lead to distortions (bi-focusing) because of the difference in magnitude in the radial and tangential directions. Note also that a linearly polarized laser beam will experience a position-dependent decomposition into radial and tangential components in the rod (see also Figure 3.1), which in effect leads to aberrations in the thermal lens. The third term is small for long and thin rods. In the end-pumped rods to be discussed in this report, we have $r_0 \approx 2$ mm and L = 10-15 mm, which means that r_0/L = 0.07-0.2. Therefore, this term would be significant if the rods were uniformly pumped However, the rods are only pumped in a narrow cylinder (typically <400 μm radius) along the rod axis, so one would expect the term to be small, and it will be ignored in the following.

2.2 Rod pumped by a Gaussian beam

In our experiments the heat is not deposited uniformly, so Equation (2.1) can not be used directly. The heat load is generated by the diode pump light distribution, which is generally quite complex and varies along the direction of propagation. In the following we will assume a Gaussian pump beam which is well collimated over the length L of the rod. If we assume that the fraction of the absorbed pump light which is converted to heat is constant, i.e. independent of the local pump intensity, and assume strictly radial cooling, we can ignore the axial variation of the heat load in the calculation of thermal lensing and birefringence. We therefore approximate the heat load (W/m^3) by an average Gaussian radial function:

$$I_h(r) = \frac{2P_h}{L\pi\omega_p^2} \exp\left[-2\left(\frac{r}{\omega_p}\right)^2\right], \tag{2.2}$$

where P_h is the total generated heat power and ω_p is the Gaussian beam radius.

It should be noted that, in general, the fraction of the absorbed power that is converted to heat is not constant, since some of the heat generating processes (e.g. upconversion) may depend on the local pump intensity. Also, some of the parameters determining the thermal lens (e.g. $\partial n/\partial T$ and k) may depend on temperature and thereby on the local pump intensity. Such effects can be taken into account using more rigorous numerical simulation models, and this will be done in the reports discussing the specific laser systems. However, a good estimate of the thermal lensing effect can be obtained in many cases by using the heat load expression (2.2) and temperature independent parameters.

Solving the radial heat conduction equation in this case leads to a non-parabolic radial temperature distribution, which means that the thermal lens can no longer be described by a precise focal length. This means that there are aberrations in the thermal lens (in addition to the aberrations caused by bi-focusing, mentioned above). There exists no analytic solution for the temperature distribution in this case. However, solutions for the derivative $\partial T/\partial r$ and second derivative $\partial^2 T/\partial r^2$ can be found:

$$\frac{\partial T}{\partial r} = -\frac{P_h}{2\pi k L r}\left\{1 - \exp\left[-2\left(\frac{r}{\omega_p}\right)^2\right]\right\} \tag{2.3}$$

$$\frac{\partial^2 T}{\partial r^2} = -\frac{P_h}{2\pi k L}\left\{-\frac{1}{r^2} + \left(\frac{1}{r^2} + \frac{4}{{\omega_p}^2}\right)\exp\left[-2\left(\frac{r}{\omega_p}\right)^2\right]\right\} \tag{2.4}$$

We observe that the second derivative $\partial^2 T/\partial r^2$ is a radially varying function, which, when inserted in the denominator of Equation (2.1), leads to a radially varying thermal focal length. Ignoring the stress-induced curvature of the rod ends we obtain the following expression for the thermal focal length:

$$f_{r,\phi}(r) = \frac{1}{\frac{P_h}{k\pi}\left\{-\frac{1}{r^2} + \left(\frac{1}{r^2} + \frac{4}{{\omega_p}^2}\right)\exp\left[-2\left(\frac{r}{\omega_p}\right)^2\right]\right\}\left(\frac{1}{2}\frac{\partial n}{\partial T} + \alpha C_{r,\phi} n^3\right)} \tag{2.5}$$

We find that the focal length has a minimum on the rod axis:

$$f_{r,\phi}(r=0) = \frac{1}{\frac{2P_h}{k\pi{\omega_p}^2}\left(\frac{1}{2}\frac{\partial n}{\partial T} + \alpha C_{r,\phi} n^3\right)} \tag{2.6}$$

Using the average value of C_r and C_ϕ, we obtain the following approximate expression for the thermal focal length on the axis of a YAG rod:

$$f[\text{mm}] \approx 5000\frac{{\omega_p}^2}{P_h}, \tag{2.7}$$

where ω_p is given in [mm] and P_h is given in [W].

The interpretation of this as a lens with a radially varying focal length is fairly obvious in the geometrical optics picture, i.e. geometrical rays may be traced by applying the focal length given by (2.5). The interpretation is less useful for propagation of real laser beams, which may cover a large fraction of the pump beam. It is however still useful to have this interpretation in mind when discussing resonator stability and its sensitivity to thermal lensing, and it will be resorted to in the analytic resonator theory presented in Section 4.

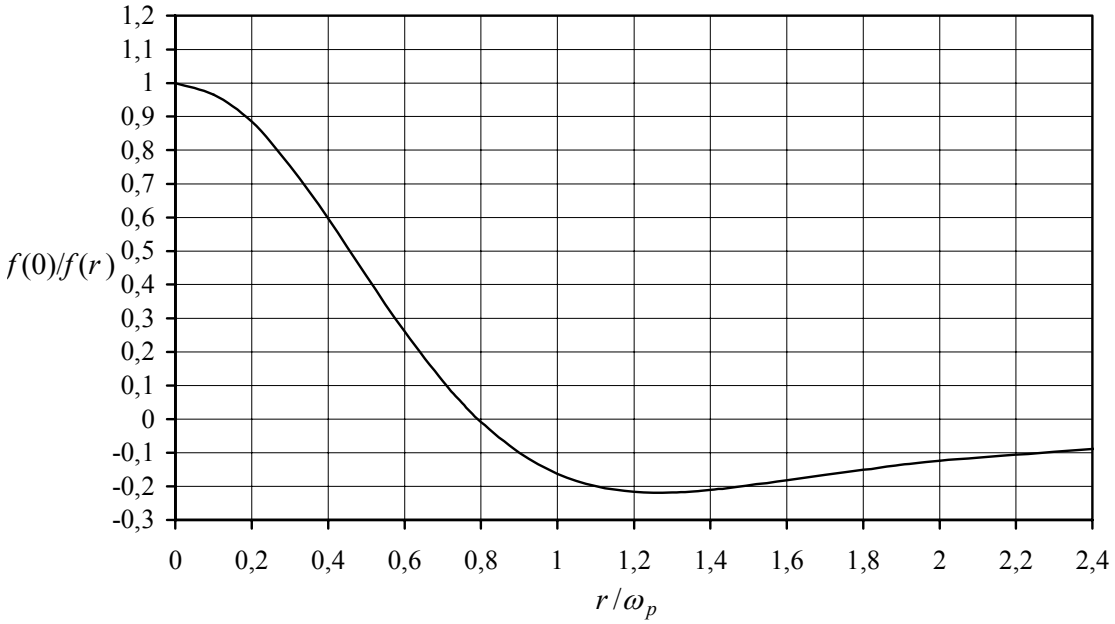

Figure 2.1: Normalized radial dependence of the thermally induced focal length, assuming a Gaussian pump distribution with beam radius ω_p.

A plot of the calculated normalized radial dependence of the inverse focal length, using (2.5) with the average value of C_r and C_ϕ, is shown in Figure 2.1. It is clear that the lens is only well defined (i.e. with a nearly constant focal length) up to a radius of about $0.2\omega_p$. The focal length changes sign from positive to negative at $r \approx 0.79\omega_p$. Normally, in order to obtain a good conversion efficiency from the pumped laser, one would prefer to match the laser mode radius to the pump beam radius ω. In that case the laser mode will experience a quite distorted thermal lens, and it is not obvious what the effect will be on the resonator stability and the laser beam quality.

The fraction of the absorbed pump power which is converted to heat may vary from about 10 % to 40 % for different rare earth ions in different crystal hosts and for different modes of operation (CW, Q-switched). Assuming a total absorbed pump power of 50 W and that 30 % is converted to heat, we obtain $P_h \approx 15$ W. If we further assume an effective beam radius $\omega_p = 0.4$ mm we find, using (2.7), that $f \approx 53$ mm on the rod axis. The thermal lens is in this case so strong that it may even lead to self-focussing of the pump beam, and thereby making the effect even stronger. The effect of thermal lensing on the stability conditions of the laser resonator will be discussed in Section 4.

It should be emphasized that the results presented above should be regarded as estimates of the magnitude of the thermal lensing effect. An accurate analysis would require a full 3-dimensional finite-element type of calculation of the temperature and stress distribution in the rod. This again would require the exact pump distribution in the rod to be taken as input to the calculation, and several iterations would probably be needed because the thermal effects would alter the pump distribution. It should also be noted that the thermal load will in general depend on how the laser is operated, even if the pump is constant. For example, a high resonator loss leads to an increased steady state population in the upper laser level, which may in turn lead to an increased heat load via increased upconversion. For the same reason, the heat load may increase under Q-switched operation as compared to CW operation. Also, the transverse distribution of the heat load may be affected by the transverse distribution of the laser field, since the laser field strength affects the upconversion rate and spontaneous emission rate.

3 STRESS-INDUCED BIREFRINGENCE

As a result of the non-uniform temperature distribution in the laser rod, there will be a non-uniform thermal expansion, which results in stress. The stress leads to deformations (strain) which in turn leads to optical birefringence in the rod via the photoelastic effect. As pointed out in the previous sub-section, this also gives a significant contribution to thermal lensing. In the case of radial symmetry, the birefringence occurs as a difference in the index of refraction between the radial and tangential polarization components of the laser field as illustrated in Figure 3.1.

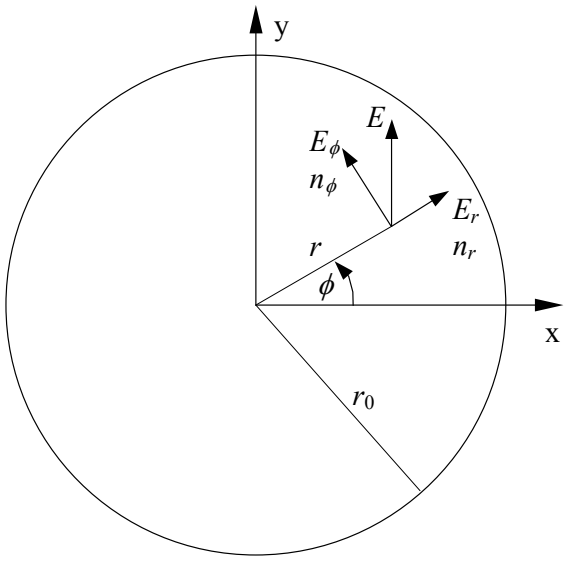

Figure 3.1: Birefringence in laser rod with radially symmetric temperature distribution

The birefringence leads to depolarization and thereby a resonator loss in resonators with polarizing elements. Analytic expressions and examples of calculations of this loss are given in Section 3.1. Section 3.2 discusses methods which can be used in order to compensate for the depolarization, and gives expressions for the improvement factor.

3.1 Depolarization losses

3.1.1 Uniformly pumped laser rod

In the case where the heat power is uniformly distributed across a rod with radius r_0, the phase shift difference between the radial and tangential polarization components for one pass through the rod becomes [3]:

$$\delta = \frac{2\pi}{\lambda}(n_\phi - n_r)L = \frac{2n^3\alpha C_B}{\lambda k} P_h \left(\frac{r}{r_0}\right)^2 = C_T P_h \left(\frac{r}{r_0}\right)^2 \tag{3.1}$$

where n_ϕ and n_r are the refractive indeces for the tangential and radial polarization components, and C_B is a parameter depending on the elasto-optic coefficients of the laser material. The other parameters were defined in connection with Equation (2.1). Using the material parameter values for YAG given in Section 2.1 and that $C_B \approx 0.01$ in YAG, we find that $C_T \approx 0.066$/W for $\lambda = 1.06$ μm (Nd:YAG) and $C_T \approx 0.035$/W for $\lambda = 2$ μm (Tm:YAG).

If the light incident on the rod is polarized in e.g. the y-direction, as shown in Figure 3.1, it will become elliptically polarized at the output. Maximum depolarization occurs along radial lines at $\phi = 45$, 135, 225, and 315 degrees, since E_r and E_ϕ have equal magnitude along these lines. The depolarization is zero along the x- and y-axis. With a polarizer in the laser resonator, the depolarization induced on the laser field after double-passing the laser rod may lead to a significant loss at the polarizer.

3.1.1.1 Top hat laser mode

In the case of a top hat laser mode with radius r_T, the loss experienced at the polarizer is [3]

$$L_T = 0.25\left\{1 - \frac{\sin(2\delta_T)}{2\delta_T}\right\}$$
$$\text{where} \quad \delta_T = C_T P_h \left(\frac{r_T}{r_0}\right)^2 \tag{3.2}$$

3.1.1.2 Gaussian laser mode

In the case where the resonator mode is Gaussian with beam radius ω we find that

$$L_G = 0.25\frac{{\delta_G}^2}{1+{\delta_G}^2}$$
$$\text{where} \quad \delta_G = C_T P_h \left(\frac{\omega}{r_0}\right)^2 \tag{3.3}$$

The calculated loss (according to (3.2) and (3.3)) as a function of the absorbed heat power, for $\lambda = 2$ μm, is shown in Figure 3.2 for 3 different resonator modes: top hat with $r_T = r_0$, top hat

with $r_T = r_0/2$, and Gaussian with $\omega = r_0/2$. In general, the loss is largest for modes occupying the largest fraction of the rod cross section. This is a consequence of the fact that the birefringence increases quadratically with radial position, as given by (3.1). The results indicate that in cases where there is a reasonable match between the pump beam and the resonator mode, the loss due to birefringence should be small for a heat power up to a few watts.

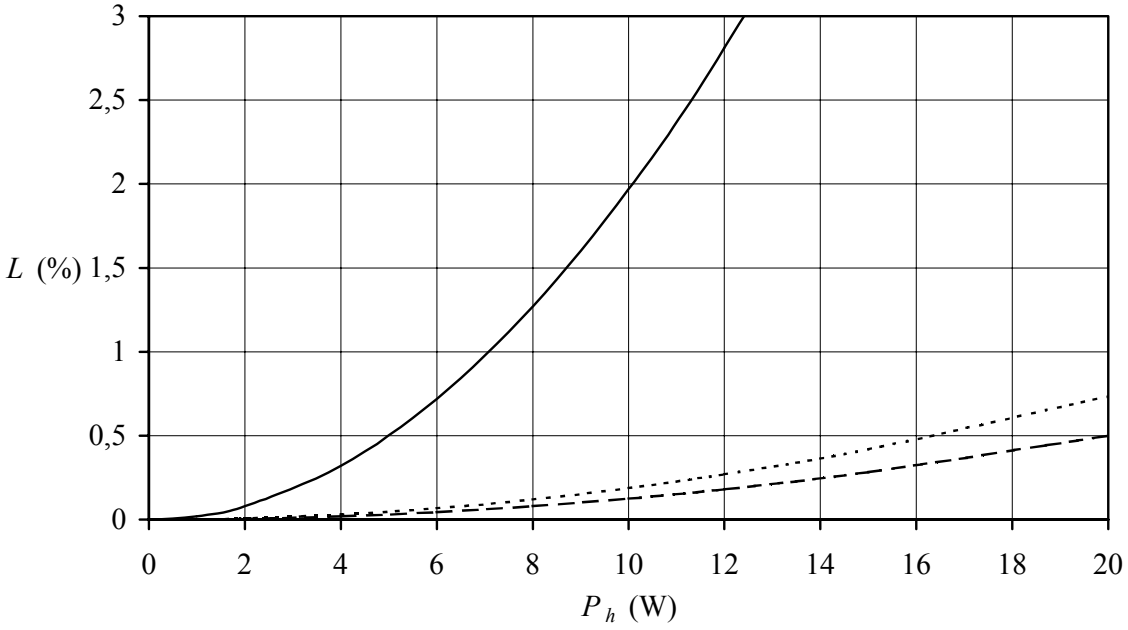

Figure 3.2: Loss due to stress-induced birefringence in a uniformly pumped YAG rod at 2 μm laser wavelength (loss at polarizer after double-pass of laser rod). Solid curve: Top hat resonator mode with radius $r_T = r_0$. Dashed curve: Top hat resonator mode with radius $r_T = r_0/2$. Dotted: Gaussian resonator mode radius $\omega = r_0/2$.

3.1.2 Gaussian pump beam and Gaussian laser mode

Analytic expressions for the depolarization loss can only be found in the case of a uniformly pumped rod, as discussed above. However, an upper bound on the depolarization loss in the case of a Gaussian pump beam can be found by calculating the loss for a uniform pump beam with the same intensity as the peak intensity of the Gaussian pump beam. Assume a Gaussian pump beam with beam radius ω_p generating a total heat power of P_h, and a Gaussian resonator mode with radius ω. The heat power per unit area in the center of the rod is $I_h = 2P_h/(\pi\omega_p^2)$. In order to find the upper bound for the loss, we assume that I_h is distributed uniformly across a rod with radius r_0, which corresponds to a total equivalent heat power in the rod of $P_{h,eq} = 2P_h(r_0/\omega_p)^2$. Using this equivalent heat power in (3.3) we obtain an upper bound for the depolarization loss:

$$L_{upper} = 0.25\frac{{\delta_U}^2}{1+{\delta_U}^2} \qquad (3.4)$$

where $\delta_U = 2C_T P_h \left(\frac{\omega}{\omega_p}\right)^2$

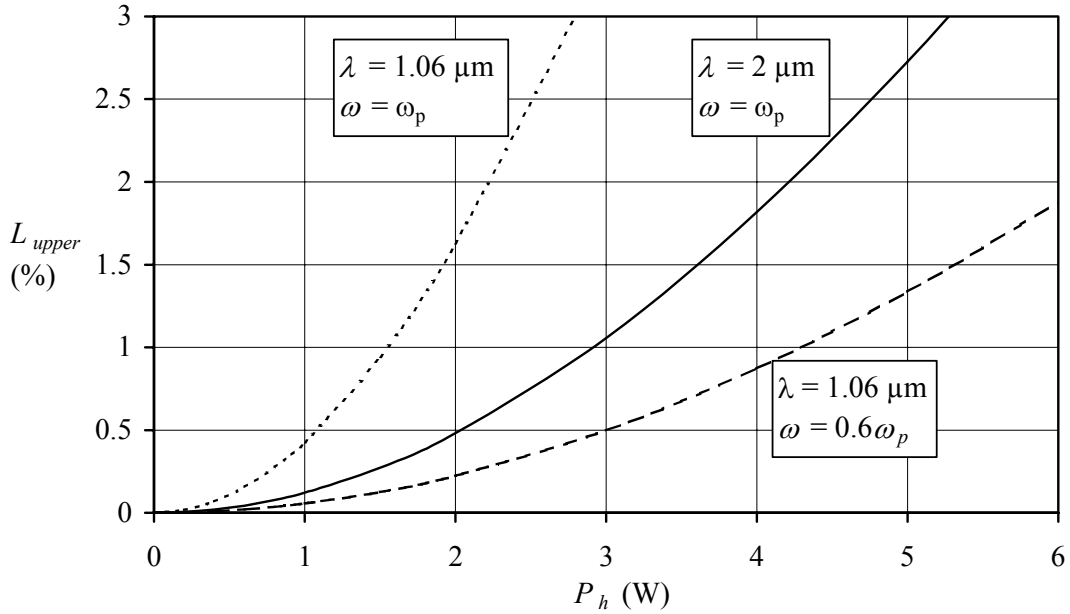

Figure 3.3: Upper limit for the depolarization loss for a Gaussian pump beam with radius ω_p and a Gaussian laser mode with radius ω, as a function of the generated heat power P_h.

Examples of the calculated upper limit for the depolarization loss are given in Figure 3.3. Note that the loss can be reduced substantially by reducing ω, since the loss is approximately proportional to ω^4. Note also that the heat load that can be tolerated for a given loss is proportional to the laser wavelength. Although the upper bound for the loss given by (3.4) is probably considerably overestimated, one may expect to see significant effects of depolarization in the power regime we will operate our lasers, with heat powers up to 15 W. In particular, in low gain lasers, such as Tm:YAG, where the output coupling is typically only 5-10 %, a loss of only a few % may lead to a substantial reduction of the output power. In the next subsection we shall therefore discuss ways of reducing the depolarization effects.

3.2 Methods of reducing depolarization losses

A common method applied to reduce the depolarization loss has been to use two identical laser rods with a 90 degrees polarization rotator between the rods [3]. In theory, this method may provide perfect elimination of the losses, since the radial and tangential polarization components are swapped between the rods. This means that the depolarization occuring in the first rod is exactly cancelled in the second rod, provided that the rods are identical and that the resonator mode has not changed between the rods.

A simpler method, which avoids the need for two laser rods, has been invented at the University of Southampton [4]. In this method, only an extra quarter-wave plate, inserted between the laser rod and the laser end mirror, is needed. The plate is aligned with one of its principal axes parallel to the main direction of polarization in the laser, usually defined by a polarizer. For a double-pass, the quarter-wave plate acts like a half-wave plate, i.e. an incoming polarization vector oriented with an angle θ relative to the principal axis of the plate is rotated by an angle 2θ after a double-pass. As discussed in connection with Figure 3.1, maximum depolarization in the laser rod occurs along lines oriented 45 degrees relative to the main polarization direction. Along these lines the radial and tangential polarization components E_r and E_ϕ (refer to Figure 3.1) are oriented 45 degrees relative to the principal axis of the waveplate, and are therefore swapped after double-passing the waveplate. Therefore, in the return pass through the laser rod, the depolarization occuring in the forward pass will be cancelled, i.e. the depolarization is cancelled along the lines where the loss was maximal without the waveplate. The correction is not complete for other directions, but the inventors of the method demonstrated experimentally in one case that it was possible to reduce a 2 % loss to a negligible level of less than 0.001 %.

3.2.1 Uniformly pumped laser rod

3.2.1.1 Top hat laser mode

We have found the following expression for the loss for a top hat laser mode with radius r_T when using a quarter-wave plate for birefringence compensation:

$$L_{T,compensated} = 0.25\left\{\frac{3}{4} - \frac{\sin\delta_T}{\delta_T} + \frac{1}{4}\frac{\sin(2\delta_T)}{2\delta_T}\right\} \qquad \text{where} \quad \delta_T = C_T P_h \left(\frac{r_T}{r_0}\right)^2 \tag{3.5}$$

The expression is valid in the case of a uniformly pumped laser rod with radius r_0 and corresponds to expression (3.2) without the waveplate. Plots of L_T and $L_{T,compensated}$ are shown in Figure 3.4 for $\lambda = 2$ μm in YAG, and assuming $r_T = r_0$, Clearly, the compensation is almost perfect up to a heat power of 15 W.

The improvement factor, defined as the loss without the waveplate divided by the loss with the waveplate, becomes:

$$\frac{L_T}{L_{T,compensated}} = \frac{8\delta_T - 4\sin(2\delta_T)}{6\delta_T - 8\sin\delta_T + \sin(2\delta_T)} \quad \rightarrow \quad \frac{80}{3\delta_T{}^2} \quad \text{for} \quad \delta_T << 1 \tag{3.6}$$

We find the improvement factor to be > 25 for $\delta_T < 1$. For $P_h = 15$ W and $r_T = r_0$, we find that $\delta_T \approx 0.53$ and $L_{T,compensated} \approx 0.05$ %.

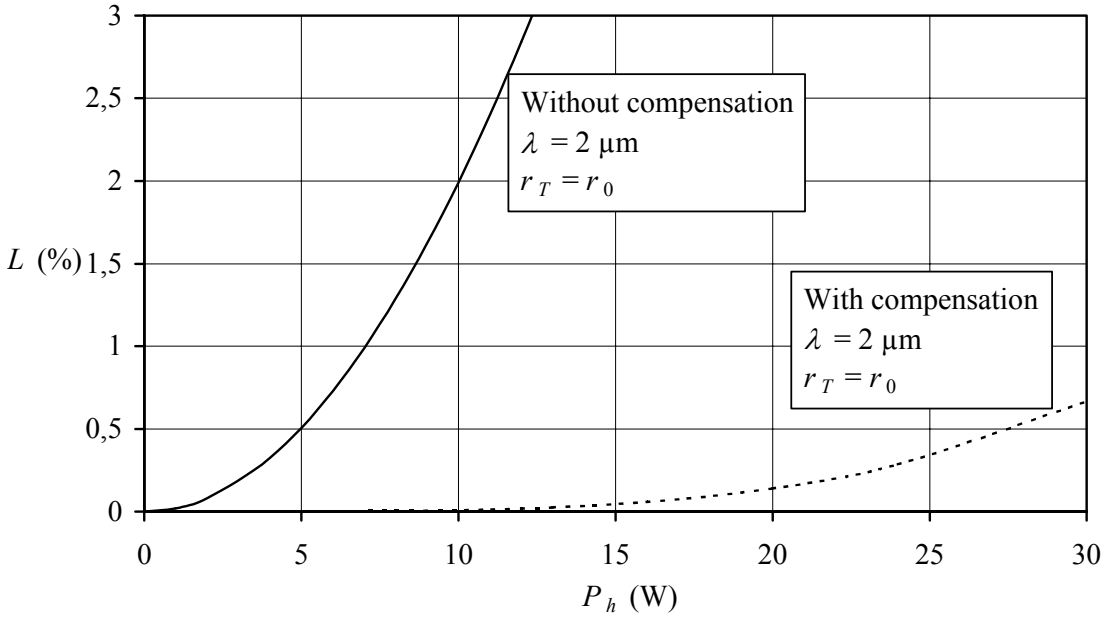

Figure 3.4: Calculated loss, using (3.2) and (3.5), for top hat laser mode in YAG laser rod, with and without the use of a quarter-wave plate for birefringence compensation.

3.2.1.2 Gaussian laser mode

In the case of a Gaussian laser mode with radius ω we find the following expression for the compensated loss:

$$L_{G,compensated} = \frac{3\delta_G^{\,4}}{16(4+5\delta_G^{\,2}+\delta_G^{\,4})}$$
$$\text{where} \quad \delta_G = C_T P_h \left(\frac{\omega}{r_0}\right)^2 \tag{3.7}$$

The expression corresponds to expression (3.3) obtained without the waveplate. The improvement factor in the case of a Gaussian laser mode becomes:

$$\frac{L_G}{L_{G,compensated}} = \frac{4(4+5\delta_G^{\,2}+\delta_G^{\,4})}{3\delta_G^{\,2}(1+\delta_G^{\,2})} \quad \rightarrow \quad \frac{16}{3\delta_G^{\,2}} \quad \text{for} \quad \delta_G << 1 \tag{3.8}$$

The improvement factor is 5 times smaller than for a top hat laser mode in the case where $r_T = \omega$. This is due to the fact that the Gaussian mode extends outside r_T, where the compensation is relatively poor. However, the compensation obtained with the quarter-wave plate is still very good for small values of δ_G. For example, for $\lambda = 2$ µm, $P_h = 60$ W and $\omega = r_0/2$, we find that $L_{G,compensated} \approx 0.26$ %.

3.2.2 Gaussian pump beam and Gaussian laser mode

In the case of a laser rod pumped by a Gaussian beam with beam radius ω_p, an upper bound for the compensated loss can be calculated by replacing r_0 with $\omega_p/(2)^{1/2}$ in (3.7). The upper bound is found by similar arguments as those used in Section 3.1.2.

4 LASER RESONATOR STABILITY CONSIDERATIONS – ANALYTIC THEORY

In this section we will discuss the laser resonator mode formation in the presence of strong thermal lensing induced by a Gaussian pump beam, as discussed in Section 2.2. As was shown in Figure 2.1, such pumping leads to a radially varying focal length with a minimum on the axis, and which changes sign from positive to negative at a distance of about $0.8\omega_p$ from the axis. As a general guide line, one would expect that in order to obtain good performance in terms of beam quality and efficiency, the laser resonator should provide a lowest order resonator mode which covers a fairly large fraction of the pump mode, and which remains stable for the range of thermal focal lengths experienced by the mode. Obviously this will become increasingly difficult for increasing pump power, due to the increasing range of thermal lens powers experienced by the resonator mode.

In order to gain physical insight in the resonator mode formation in the presence of thermal lensing, we will first make a simplified analysis using standard analytic Gaussian resonator mode theory. This analysis can be used as a guide line for the resonator design. Later, in Section 5, we will give examples of results obtained with a rigorous numerical simulation of an end pumped Nd:YAG laser, and compare the results with the expectations from the analytic theory.

4.1 Choice of resonator

There are a number of possible choices of laser resonator, but the simplest resonator to realize and to analyze is the 2-mirror resonator shown in Figure 4.1.

The laser rod is intentionally placed as close as possible to the pump input mirror in (a). As a result of the pumping, the rod acquires a thermal lens. If the rod is short compared with the thermal focal length, f, and the resonator length, L, the resonator can be approximated by the simplified resonator shown in (b), where the rod is replaced by a thin lens with focal length, f, placed adjacent to the input mirror. As discussed above, the thermal focal length is in reality a radially varying function, but in order to gain insight we will analyze the behaviour of the resonator as a function of the focal length of a simple thin lens.

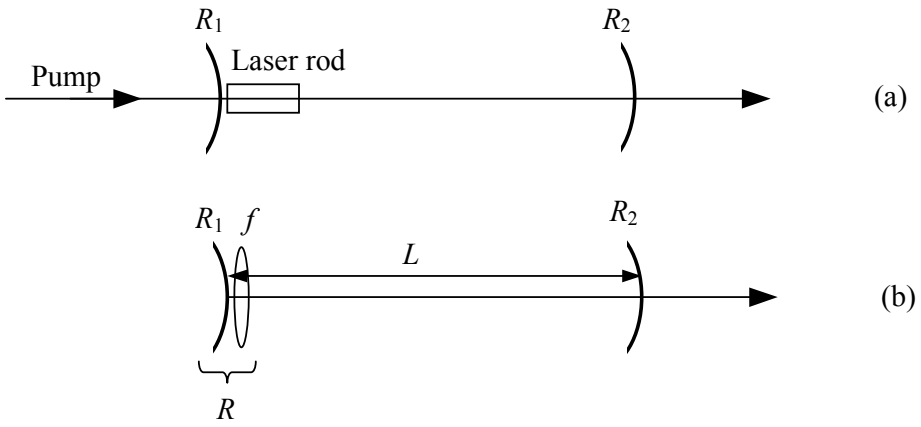

Figure 4.1: (a): End-pumped laser with 2-mirror resonator.
(b): Simplified equivalent resonator where the laser rod is replaced by a thin lens with focal length f placed adjacent to the pump input mirror.
R_1 and R_2 are radii of curvature, which are defined to be positive if the center of curvature is on the left side of the mirror.

With the simplified resonator we observe that a convex input mirror can be used to compensate for thermal lensing. Together, the input mirror and the lens form an equivalent mirror with radius of curvature, R:

$$R = \frac{fR_1}{f - R_1} \tag{4.1}$$

If, for example, R_1 is chosen equal to f, the equivalent mirror is flat, and the resonator is stable as long as $R_2 > L$.

4.2 Resonator stability analysis

The general stability condition for this resonator is given by the familiar expression:

$$-1 < \left(1 + \frac{L}{R}\right)\left(1 - \frac{L}{R_2}\right) < 1 \tag{4.2}$$

Note that we define the radius of curvature to be positive when the center of curvature is at the left side of the mirror.

Combining (4.1) and (4.2), we find that the resonator remains stable for values of f within the following range:

$$\frac{R_1 L}{R_1 + L} < f < \frac{(R_2 - L)R_1}{R_2 - L - R_1} \tag{4.3}$$

The minimum value of f corresponds to a situation where the center of curvature of the equivalent input mirror is positioned at the output mirror, i.e. $-R = L$. Note that this minimum value is independent of R_2. As the resonator approaches this stability border, the resonator mode becomes strongly focussed on the output mirror, which could lead to serious problems with optical damage, particularly in Q-switched mode of operation. The maximum value of f corresponds to a situation where the centers of curvature of the equivalent input mirror and the output mirror coincide (concentric resonator). In this case the resonator mode size becomes infinitely large at both mirrors. It is therefore generally advisable to choose mirror radii and resonator length such that, for the relevant range of focal lengths, the resonator is closer to the upper stability border than the lower border. In addition, one should seek to obtain a lowest order resonator mode size at the lens, which provides a suitable filling of the pump beam size.

Plots of the minimum and maximum values of f (f_{min} and f_{max}) as functions of R_1 are given in Figure 4.2 for a number of different values of R_2, and assuming $L = 80$ mm. Note that f_{min} is the same for all R_2 for a given value of R_1. f_{min} is a slowly varying function of R_1 (approaches R_1 for $R_1 << L$ and approaches L for $R_1 >> L$). The curves for f_{max} depend strongly on R_2, and the stability range for a given value of R_1 increases for decreasing (positive) values of R_2. This might seem to indicate that it ought to be advantageous to us a small value of R_2. However, a smaller value of R_2 also leads to a smaller resonator mode radius at the lens, i.e. in the laser rod (see below), which may lead to a less favourable overlap with the pump mode. A careful analysis of this overlap should be performed in order to optimize the performance in terms of efficiency and beam quality.

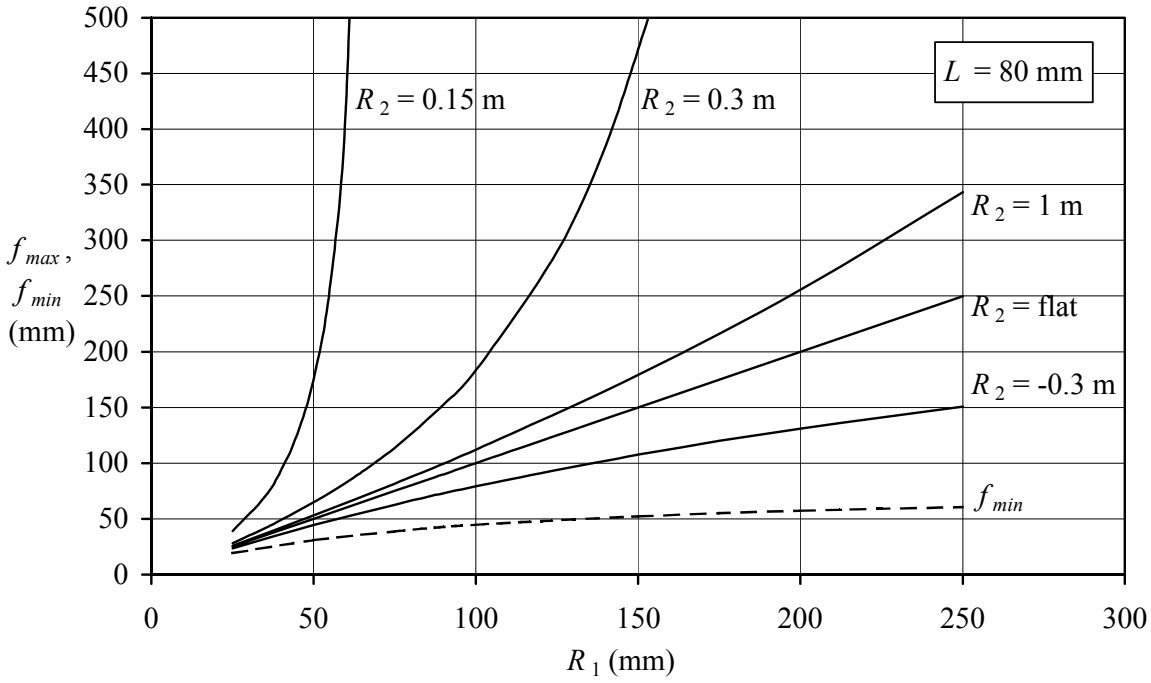

Figure 4.2: Plots of the minimum and maximum values of the focal length f, given by (4.3). f_{min} is shown by the dashed curve, f_{max} by solid curves for different values of R_2.

4.3 Resonator mode size

For given values of R_2, L, and the laser wavelength λ, there is a minimum possible value of the resonator mode radius ω_f at the lens. Curves showing this minimum value as a function of R_2, are given in Figure 4.3, for L = 80 mm, λ = 1.06 µm (Nd:YAG), and λ = 2.015 µm (Tm:YAG). It should be noted that the mode diameter is proportional to the square root of the wavelength. For this reason, it generally easier to obtain good overlap with large pump beams at 2 µm than at 1 µm.

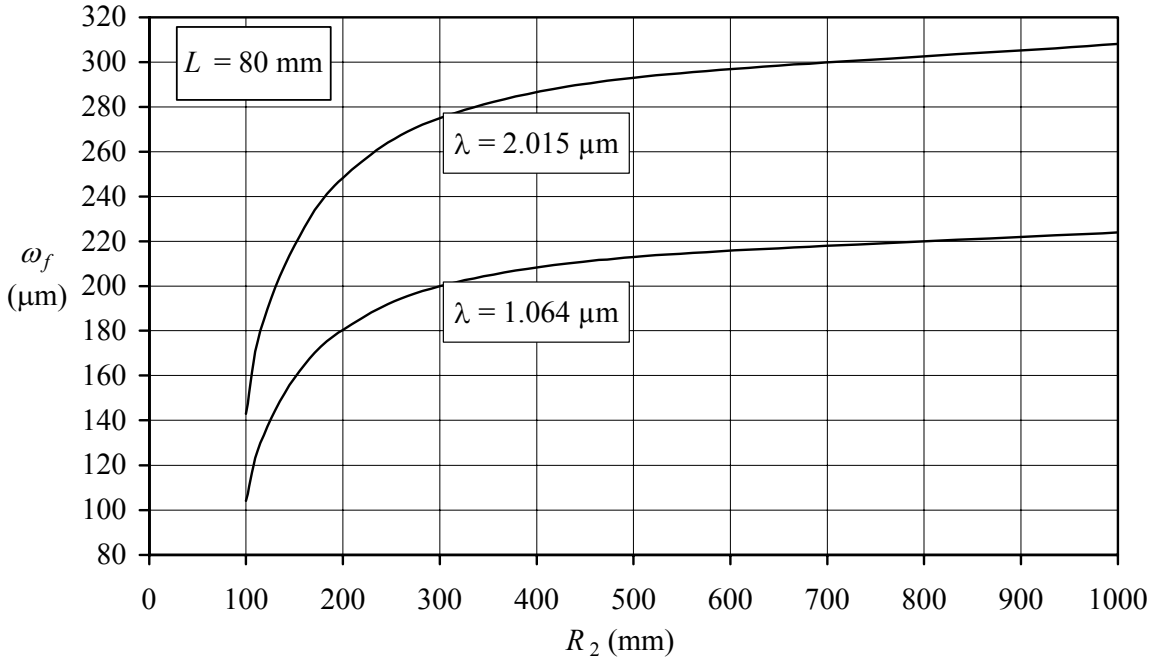

Figure 4.3: Minimum value of the resonator mode radius ω_f at the lens as a function of R_2.

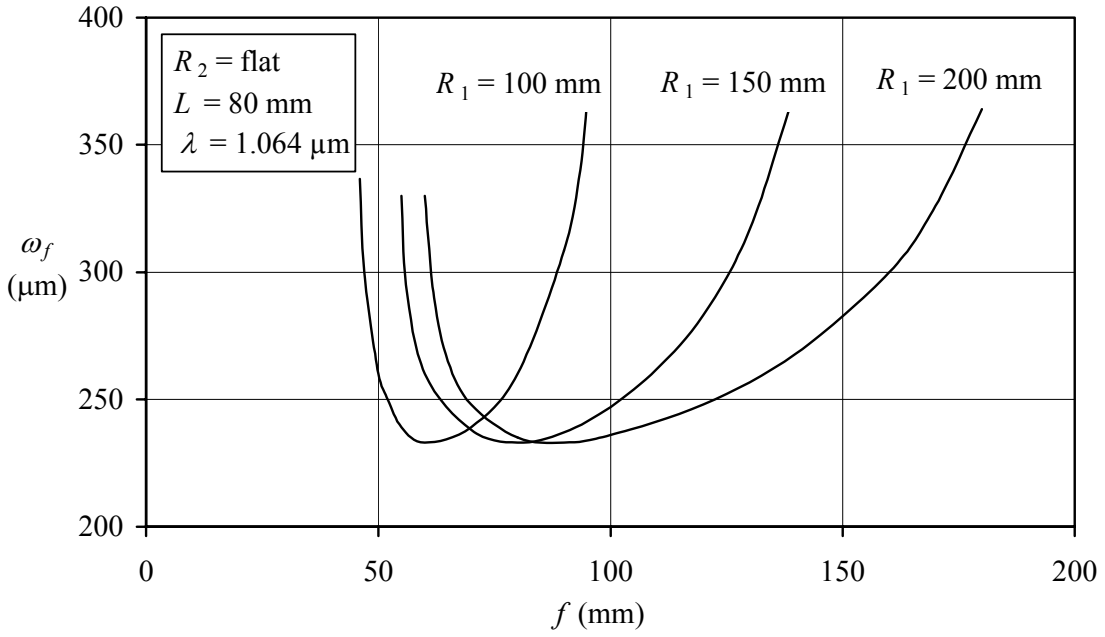

Figure 4.4: Resonator mode radius at the lens as a function of f.

Figure 4.4 shows the calculated resonator mode radius ω_f at the lens as a function of f for R_1 = 100 mm, 150 mm, and 200 mm, in the case of a flat output mirror, L = 80 mm, and λ = 1.064 μm. Note that the minimum value is the same for all values of R_1. It can be observed that the mode radius increases rapidly as the focal length approaches the stability boundaries given in Figure 4.2. As discussed earlier, one should avoid approaching the lower stability boundary, f_{min}, where the resonator mode acquires a focus at the output mirror. As was also discussed earlier, the thermal lens induced by a Gaussian pump beam has minimal focal length $f(0)$ on the axis. Therefore, for a given value of $f(0)$, one should choose a value of R_1 such that $f(0)$ is well above the lower stability boundary. For example, if $f(0)$ = 50 mm, one should choose R_1 < 100 mm in Figure 4.4 in order to achieve this. In order to determine the optimal value of R_1, one will also have to consider the degree of overlap between the pump beam and the resonator mode, as discussed in Section 5.

5 NUMERICAL SIMULATIONS

In order to predict the performance of the laser in more detail and to optimize the resonator, it is necessary to perform quite rigorous and time-consuming numerical simulations. This can most effectively be performed after a choice of approximate resonator parameters has been made, based on the guide lines provided by the analytic theory discussed in Section 4. An advanced numerical laser simulation model has been developed at FFI for this purpose (see below). Some examples of results obtained using this model to simulate the performance of end-pumped lasers are given in this section.

5.1 Numerical model

The simulation model is based on the same principles as the model reported in references [5] and [6]. Beam propagation in the resonator is handled by a FFT-based algorithm. Gain and thermal lensing are handled by a split-step method, with rate equations for the laser gain and population dynamics. The required number of split-steps in the gain medium depends both on the type of gain medium (especially whether there are competing nonlinear processes involved, such as upconversion) and on the variation of the pump beam and laser resonator mode along the gain medium. In the simulations presented below of a Nd:YAG laser with a short laser rod, we use only 2-4 split-steps. In the case of two steps, the gain and the thermal lens are collapsed into two planes at positions $z = 1/4L$ and $z = 3/4L$, where L is the length of the rod. The model operates with time slices corresponding to the round trip time of the laser. The number of temporal samples per time slice equals the number of longitudinal modes in the simulation. The model can handle multiple longitudinal modes, but only a single mode is used in the present simulations. The pump beam is propagated by the same methods as the laser beam, but it is absorbed instead of being amplified in the rod.

The characteristic time constants describing the population dynamics in a CW-pumped solid state laser can be very long compared to the round trip time. The upper laser level life time in the different laser material is in the range of 0.2-10 ms, which results in a relaxation oscillation period of typically a few μs and a time to reach steady state of several ms. Running such long simulations with a time resolution of one round trip time is not practical. We avoid the long

simulation time by artificially changing the time constants of the population dynamics in the rate equations. Specifically, the doping concentration and the life times are divided by the scaling factor κ, and the absorption and emission cross-sections as well as the upconversion rate are multiplied by κ. The transformed equations have the same steady-state solution, but this solution is reached much faster and with less relaxation oscillations. We have checked the consistency of the steady-state solution by varying κ by up to a factor of 1000. Typical values of κ used in the simulations were in the range of $10^4 - 10^6$, the highest values correspondking to lasers with the longest upper laser level life times. We found that, in order to avoid relaxation oscillations, it was sometimes helpful to turn the pump power on gradually with a suitable ramp (typically100 ns in the case of Nd:YAG).

The temperature distribution in the rod is computed by iteration of two separate programs. The laser model first computes the distribution of absorbed pump power in the rod. This is fed into a separate thermal program which computes the temperature distribution from the given absorbed power distribution and boundary conditions. The resulting temperature distribution is fed back into the laser model, and the process is iterated until a stable solution is found. The contributions to the heat load are the quantum defect of the laser process and upconversion. All the energy of the upper level ions lost by upconversion is assumed to be converted to heat. The contribution from upconversion implies that the heat load can be much greater when the laser is not running than when it is running. The temperature distribution is used for calculating thermal lens effects in the laser model. Only the effect caused by the temperature dependence of the refractive index is included, not thermal birefringence and bulging of the rod ends.

5.2 Nd:YAG laser – optimization of beam quality and output power

As a first example, we consider the optimization of beam quality and output power from a Nd:YAG laser pumped from one end (as in Figure 4.1) by a Gaussian beam with pump beam radius $\omega_p = 0.4$ mm and a total pump power $P_{pump} = 50$ W at 806 nm. It is commonly assumed that about 25 % of the pump power is converted to heat in diode-pumped Nd:YAG lasers. Making this assumption, we calculate, using (2.7), a thermal focal length on the axis of $f(0) \approx 68$ mm. It should be noticed, however, that in some reports in the literature the fraction of the pump converted to heat has been be as large as 35-40 % [7],[8]. The consequences of such an increased heat-load will be studied in Section 5.3. Figure 5.1 shows the calculated beam quality and output power as a function of R_1 for a flat output coupler with transmittance $T_2 = 50$ %, and $L = 80$ mm. It is found that the best combination of beam quality and output power is obtained for $R_1 \approx 130$ mm, which is indeed within the range that we would predict by studying Figures 4.2 and 4.4. The value of ω_f for $f(0) = 68$ mm and $R_1 = 130$ mm is about 240 μm (se Figure 4.4), i.e. about 60 % of the pump beam radius. The mode radius obtained from the numerical simulation is slightly larger (about 66 % of the pump radius), but still a substantial fraction of the resonator mode is located inside the central part of the pump beam where the thermal lens is reasonably well defined (see Figure 2.1). The wings of the resonator mode experience a much larger thermal focal length (outside the stability boundary), and thereby a high diffraction loss, which helps to prevent multimode operation.

In fact, the large aberrations imposed on the wings of the resonator mode seem, under certain conditions, to represent a kind of soft aperture, which helps to clean up the beam and ensure a

high beam quality. Fortunately, these optimal conditions with respect to beam quality also seem to provide very high conversion efficiency. Only a marginal increase in output energy can be obtained by increasing R_1 above the optimal value in Figure 5.1, and this increase occurs at the expense of a significantly poorer beam quality.

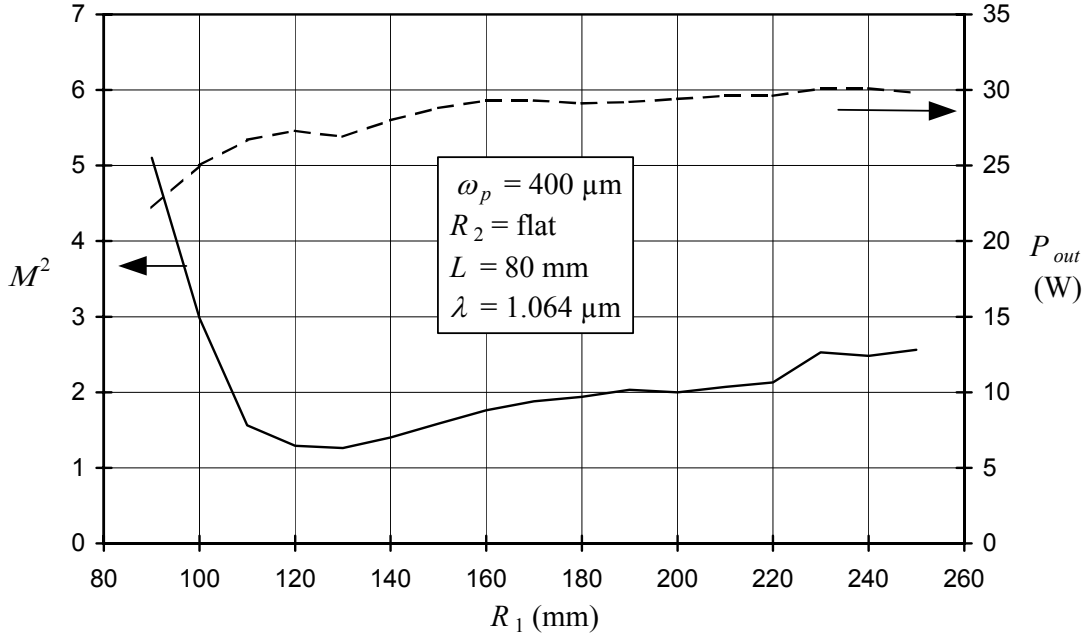

Figure 5.1: Beam quality and output power as a function of R_1.

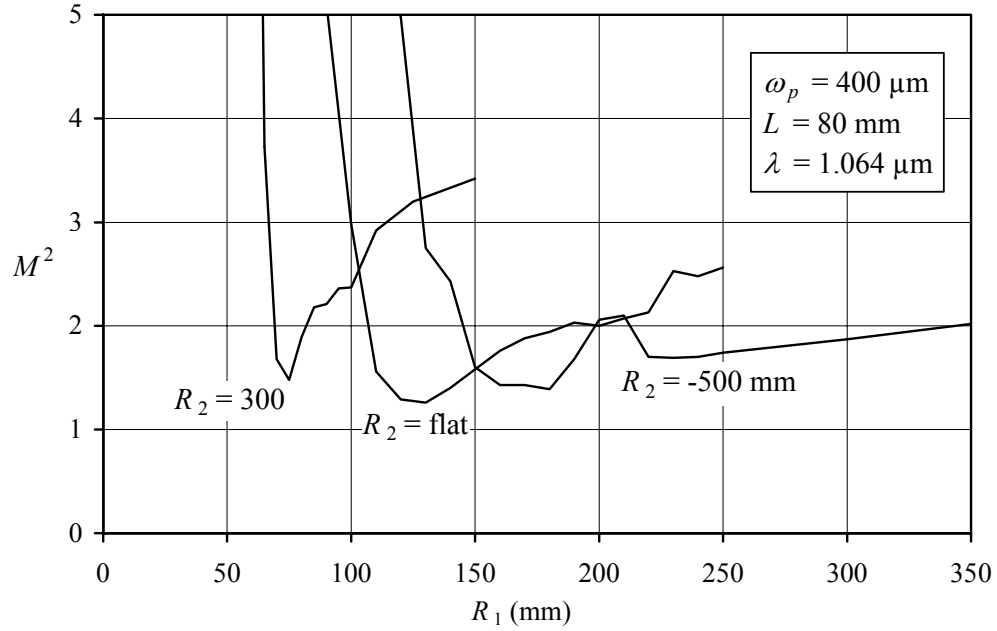

Figure 5.2: Beam quality as a function of R_1 for R_2 = 300 mm, ∞, and –500 mm.

Further examples of the dependence of the beam quality on R_1 are given in Figure 5.2, for different values of R_2. It is seen that the optimal value of R_1 decreases when R_2 varies from negative to positive. This is a consequence of the change in the upper stability boundary for the thermal focal length (see Figure 4.2) and the need for the thermal focal length to be fairly close to that boundary, in order to obtain a sufficiently large resonator mode size and thereby obtain a suitable filling of the pump mode, which ensures the beam clean-up discussed above. This becomes even more critical due to the fact that the minimum mode radius in the rod decreases as R_2 is changed from negative to positive (see Figure 4.3), making it more difficult to obtain the required filling of the pump mode.

5.3 Anomalous behaviour outside the resonator stability region

The results obtained in the examples shown above are in accordance with the expectations provided by the analytic theory in Section 4. We have found, however, that the detailed numerical simulations sometimes provide quite unexpected results. This was the case when the pump beam radius used in Figures 5.1 and 5.2 was reduced from 400 μm to 300 μm. The thermal focal length on the rod axis, $f(0)$, then decreased to about 38 mm, which is below the lower resonator stability limit for values of R_1 above 70 mm (see Figure 4.2). By reducing R_2 to 200-300 mm and choosing a value of R_1 around 50-55 mm, it was possible to achieve a sufficient stability margin to obtain good beam quality, as shown in Figure 5.3. Increasing R_1 above this value did initially (as expected) lead to a poorer beam quality, but for sufficiently large R_1 the beam quality improved and became extremely good for R_1 values of 140-200 mm, where the thermal focal length on the rod axis is far below the lower stability boundary. It appears that, under these conditions, there exists a quite well behaved resonator eigenmode, which is not properly described by ordinary Gaussian resonator mode theory. It should be noted that under these conditions the stability range towards large focal lengths is very large, which may help to stabilize the wings of the resonator mode. Also, since the pump beam in this case is quite narrow, this may help to prevent multi-mode operation. Nevertheless, it is surprising that the resonator can tolerate the very large optical aberrations imposed by the thermal lens, and that a high-quality and low-loss resonator mode can develop under these conditions.

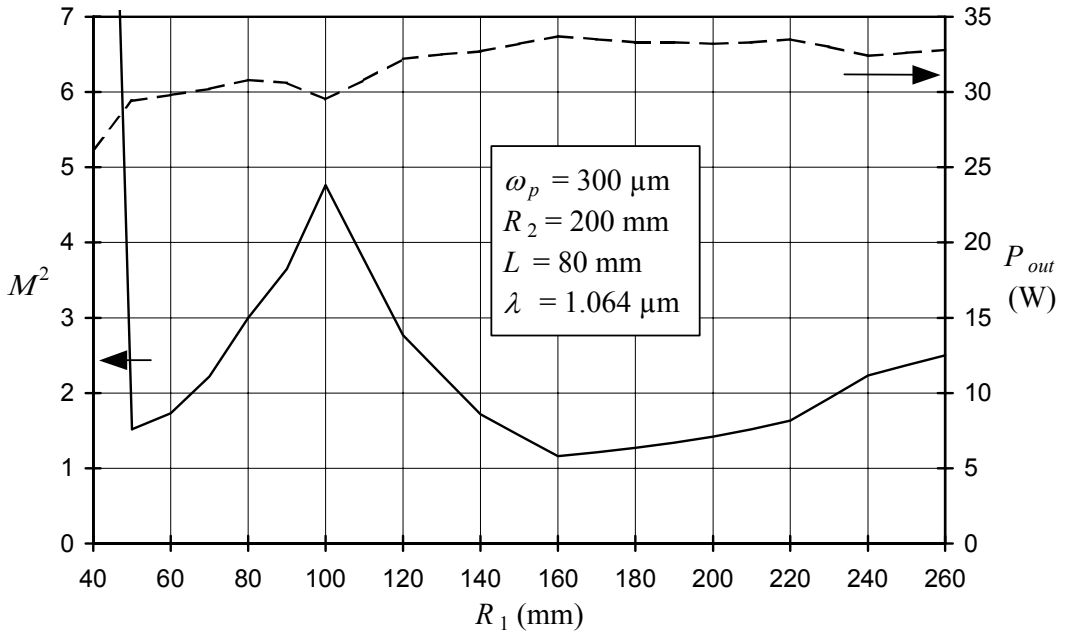

Figure 5.3: Beam quality and output power as a function of R_1 for 300 µm pump beam radius. In this case the thermal focal length is below the lower resonator stability boundary for R_1 > 70 mm.

The numerical analysis is also important in order to show the sensitivity of the performance characteristics to parameter variations. For example, Figures 5.1 and 5.2 show that a variation in R_1 may lead to a substantial change in beam quality, but little change in output power. Because the magnitude of the thermal focal length is so critical for the resonator stability conditions, one should also expect that for a given laser, with fixed resonator mirrors and pump spot size, the beam quality may depend critically on the pump power. An example of this is given in Figure 5.4. The output mirror and pump spot size in this case are the same as in Figure 5.1, and we have chosen a fixed R_1 of 120 mm, which gave the best beam quality in Figure 5.1 for a pump power of 50 W. As expected, the best beam quality is obtained for 50 W pump power. The beam quality becomes very poor for lower pump powers, where the thermal focal length on the axis, $f(0)$, approaches the upper resonator stability limit. For higher pump powers, as $f(0)$ approaches the lower stability limit, the beam quality becomes gradually poorer. However, for pump powers in the range of 90-100 W, which corresponds to a value of $f(0)$ well below the lower stability limit, the beam quality again becomes very good, and the efficiency reaches a maximum. This case corresponds to the situation shown in Figure 5.3, where the beam quality reached a second optimum for $R_1 \approx 160$ mm. Also in that case, $f(0)$ was well below the lower stability limit.

The simulated beam profiles at the output coupler are shown in Figure 5.5 for pump powers of 50 W and 95 W, respectively, corresponding to the two regions with high beam quality in Figure 5.4. It can be observed that for 95 W pump power the beam is strongly focussed on the output coupler with an intracavity intensity of about 0.7 MW/cm^2.

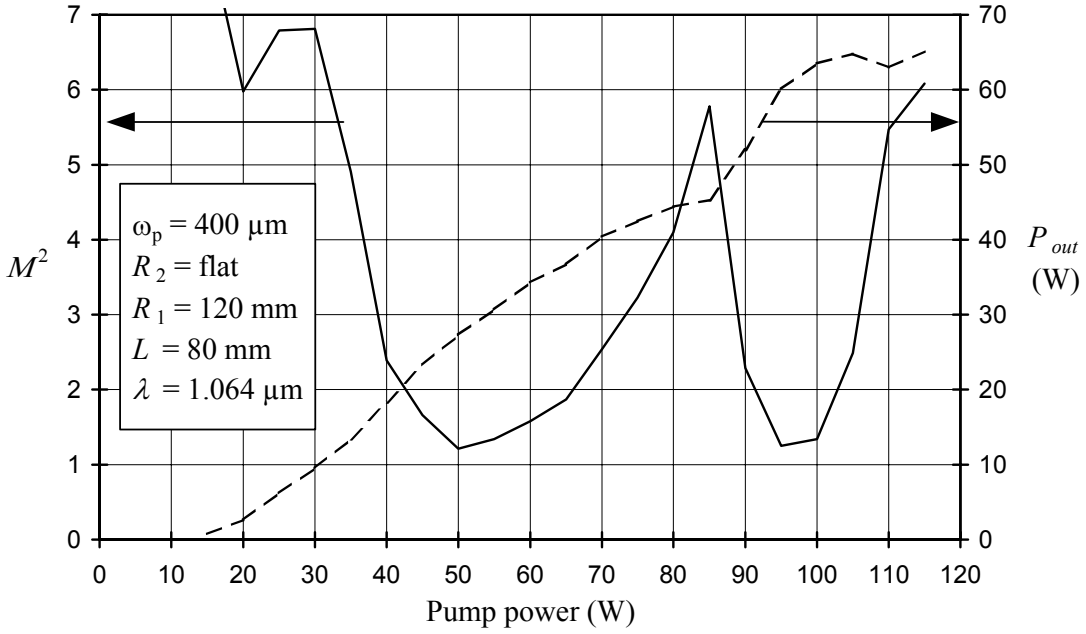

Figure 5.4: Beam quality and output power as a function of the pump power for a fixed value of R_1 (120 mm). Other parameters are as in Figure 5.1. Note that R_1 = 120 mm gave the best beam quality in Figure 5.1, with a fixed pump power of 50 W.

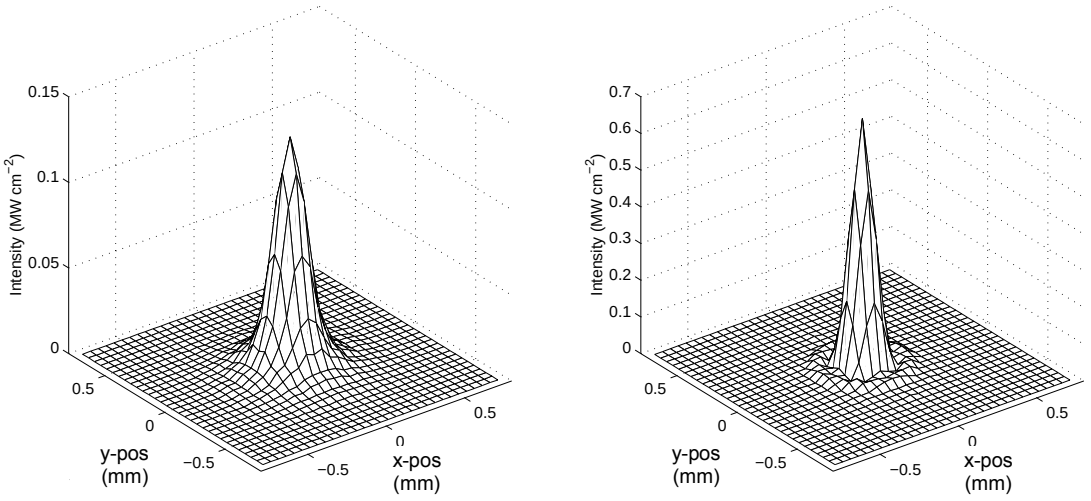

Figure 5.5: Beam profiles at the output coupler for 50 W (left) and 95 W (right) pump power.

It should be noticed that the simulation results may depend quite critically on the assumptions made for important parameters in the laser medium, which are not always known with high accuracy. For example, in the case of Nd:YAG, there have been reports with a fairly large range of values of the fraction of the absorbed pump power which is converted to heat [7],[8]. As pointed out in Section 5.2, it is commonly assumed that about 25 % of the pump is converted to heat, which corresponds to the quantum defect between the pump and laser

photons. A larger fraction of heat may be caused by different processes, such as upconversion processes, nonradiative relaxation from the upper laser level, and nonradiative relaxation to the ground state from the energy level exited by the pump radiation. The latter process implies that there will be less than 1 ion exited to the upper laser level per absorbed pump photon, and is generally referred to as a reduced pump quantum efficiency. This leads not only to increased thermal lensing, but also to reduction of the laser gain and conversion efficiency. We have made a simulation similar to that shown in Figure 5.4, but assuming a pump quantum efficiency of 85 %. This means that the fraction of the pump converted to heat increases from 25 % to about 37 %. We have therefore correspondingly reduced the radius of curvature R_1 of the pump input mirror from 120 mm to 80 mm in order to obtain an optimal thermal lens compensation at about 50 W pump power, as in Figure 5.4. The results in terms of output power and beam quality are shown in Figure 5.6. The general behaviour is the same as in Figure 5.4, but the regions of pump power yielding high beam quality are narrower, and the output power is lower, since a smaller fraction of the pump power results in excitation to the upper laser level. This results in a power reduction from 28 W to 22 W at 50 W pump.

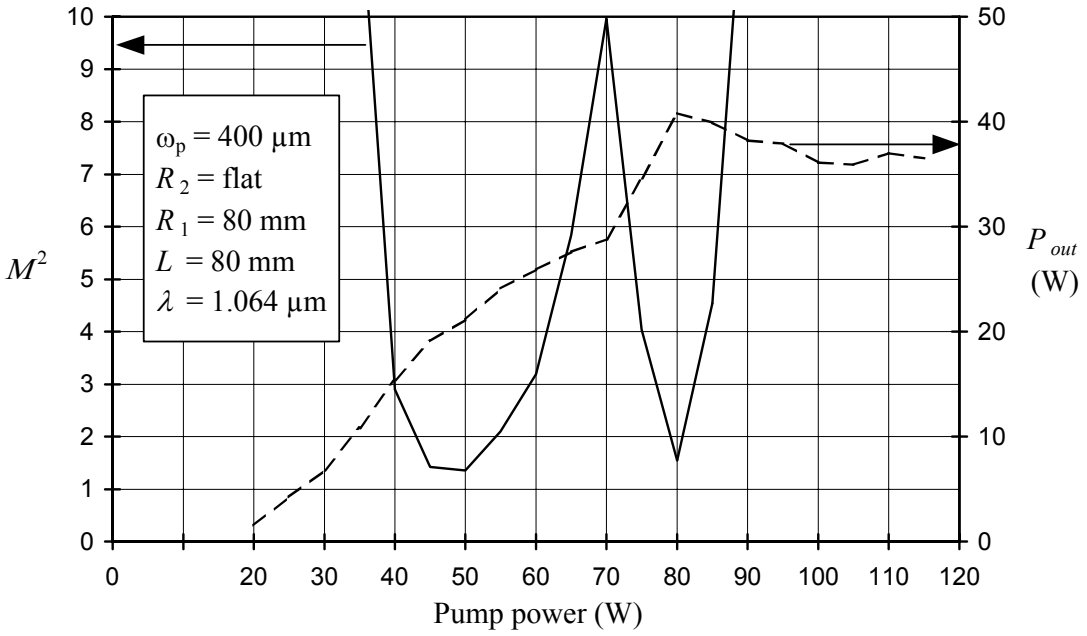

Figure 5.6: Beam quality and output power as a function of the pump power for a fixed value of R_1 (120 mm). Other parameters are as in Figure 5.1. Note that R_1 = 120 mm gave the best beam quality in Figure 5.1, with a fixed pump power of 50 W.

5.4 Dependence on laser wavelength

It should also be noted that lasers with a larger wavelength (e.g. 2 µm in Tm:YAG) will be considerably more tolerant to the aberrations imposed by the thermal lens. The simulations have shown that this can lead to a significantly improved beam quality. Contributing to this in some cases is also the fact that the resonator mode is larger for a larger laser wavelength (see Figure 4.3). An illustration of this effect is given in Figure 5.7, where the simulated beam quality and output power are shown for conditions identical to those of Figure 5.4, except that

the laser wavelength has been increased from 1.064 μm to 2 μm (i.e. the gain, fractional heat load, etc, are the same as in Figure 5.4).

Compared with the results in Figure 5.4, the most striking difference is the good beam quality at low pump powers. Due to the larger wavelength, the laser is apparently much more tolerant to the phase aberrations imposed by the thermal lens. This is even more striking, considering the fact that the resonator mode is much wider for 2 μm wavelength (see Figure 4.3), meaning that the mode will cover the parts of the thermal lens where the aberrations are strongest. It is rather surprising that the beam quality is still good at pump powers as low as 20 W. At this power the thermal focal lens on the rod axis is about 170 mm, which is above the maximum value required for a stable resonator (see Figure 4.2). The only explanation we can think of is that the effect of gain guiding is sufficient to ensure resonator stability. We also observe that the beam quality remains good up to a higher pump power than in Figure 5.4. The high-beam-quality region around 100 W pump power observed in Figure 5.4 is displaced to about 135 W in this case. The shift is probably due to the difference in the resonator mode size. The output power is generally a factor of 2 lower than in Figure 5.4, due to the lower laser photon energy.

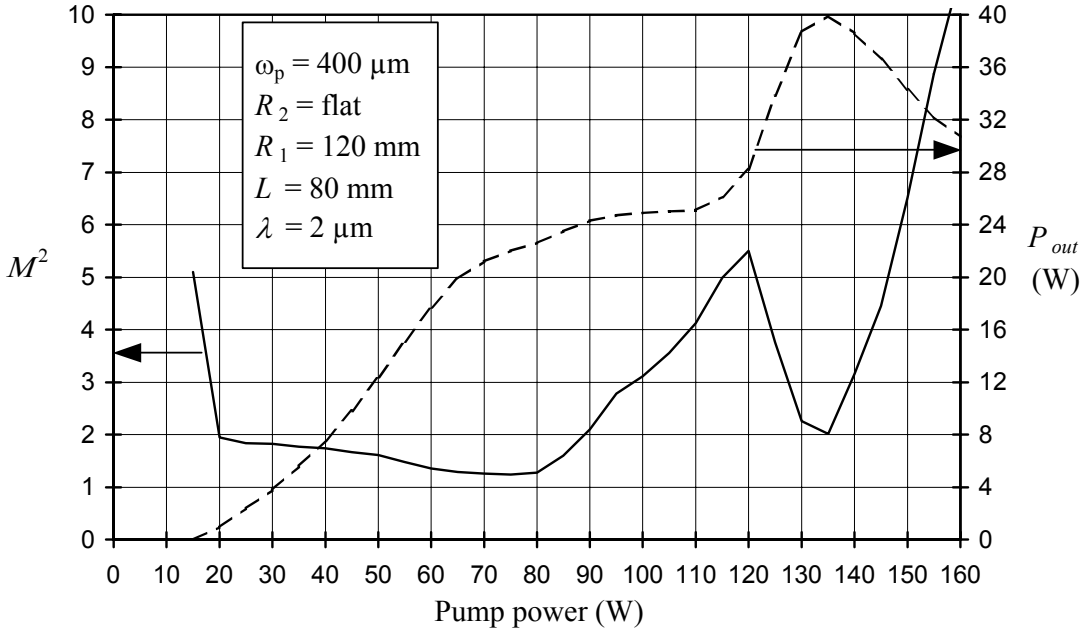

Figure 5.7: Beam quality and output power as a function of the pump power for 2 μm laser wavelength. Other parameters are identical to those used in Figure 5.4.

5.5 Other considerations

In some of the 2 μm laser systems, such as Tm:YAG, the beam quality may also be improved by the low gain, which may prevent higher order modes from reaching threshold. Contributing to this is also the fact that Tm:YAG is a 3-level laser system. In such systems, the laser mode will experience absorption outside a certain beam radius, which may also help to clean up the beam.

In general, due to the many variable parameters involved in both the resonator and the gain medium, it is not possible to predict in detail the optimal choice of parameters by a simple analytic analysis. Therefore, numerical simulations of the type discussed above have to be performed for each specific laser type, and for each set of operating conditions. As we have seen in Figures 5.3 and 5.4, this may also unveil quite surprising laser behaviour. Finally, it should be remarked that, even with numerical simulations, it is not feasible to explore the entire parameter space in detail. It will therefore be necessary both to use some of the guide-lines from Section 4 and experience from simulation examples like those presented above, in order to restrict the range of parameter values to be explored.

6 CONCLUSIONS

From the analysis given in this report, it is obvious that the operational characteristics of high-power end-pumped solid state lasers are to a large extent governed by the influence of thermal effects, such as thermally induced lensing and birefringence. The thermal lens in an end-pumped laser differs, in general, from an ideal thin lens in the sense that the focal power varies as a function of radial distance form the laser rod axis, and even changes sign from positive to negative outside a certain radius. For pump powers in the range of 10s of watts and pump diameters less than 1 mm, this represents a strongly aberrated lens with a focal length of a few cm on the axis. Estimates of the lens power and aberrations were given by Equations (2.6-2.7) and Figure 2.1.

The radial temperature distribution in the laser rod also leads to stress, which induces birefringence, and thereby a loss, if the resonator contains a polarizing element. Analytic expressions for the magnitude of this loss for different pump and resonator modes were given in Section 3. As was shown in Figure 3.3, the resulting loss may be up to several % for only a few watts of heat power, and the loss increases for decreasing laser wavelength. In order to avoid clamping of the laser output at high pump power, it is therefore necessary to find methods of compensating for the birefringence, and one simple and effective method, which virtually eliminates the loss, was discussed in Section 3.3.

The resonator parameters must be chosen carefully in order to ensure that the resonator will tolerate the range of thermal focal powers experienced by the resonator mode, and in order to ensure a suitable spatial overlap between the pump beam and the resonator mode. The latter is essential in order to obtain high beam quality and conversion efficiency. An analytic treatment of resonator stability and mode size was given in Section 4. Figures 4.2-4.4 may serve as guide lines for the choice of resonator parameters. However, a numerical analysis is required in order to predict the laser performance in more detail. Examples of such simulations of a Nd:YAG laser were given in Section 5. These simulations show that the analytic theory provides fairly good guide lines for the choice of resonator parameters in many cases, but there are also some surprising results which were not predicted. In particular, we found that exceptionally high beam quality and conversion efficiency may be achieved in some cases, even if the thermal focal length on the laser rod axis is far below the lower limit for a stable resonator.

The simulations predict, in the case of a Nd:YAG laser, that with 50 W pump power and an optimal choice of resonator parameters, there is potential for at least 20 W laser output power with a beam quality of M^2 <1.5.

Finally, it should be remarked that even the numerical simulations discussed above can not be expected to predict in detail the performance of an experimental laser, since there will always be uncertainties both in material parameters and experimental parameters. Approximations made in the numerical model may also contribute to this uncertainty.

References

[1] G Rustad, E Lippert, and K Stenersen (2001): Beam shaping of high-power laser diodes, FFI/RAPPORT-2001/02647, Forsvarets forskningsinstitutt (Approved for public release)

[2] W A Clarkson and D C Hanna (1996): Two-mirror beam-shaping technique for high-power diode bars, *Optics Letters*, Vol 21, pp 375-377

[3] W Koechner (1999): Solid-State Laser Engineering, Fifth Edition, Chapter 7.1, *Springer Series in Optical Sciences,* Vol 1

[4] W A Clarkson, N S Felgate, and D C Hanna (1999): Simple method for reducing the depolarization loss resulting from thermally induced birefringence in solid-state lasers, *Optics Letters*, Vol 24, pp 820-822

[5] H Ajer, S Landrø, and K Stenersen (1994): Numerical simulations of diode side-pumped Q-switched Nd:YAG laser oscillators and amplifiers with rod and zigzag slab crystal geometry, *OSA Proceedings on Advanced Solid State Lasers*, Vol 20, pp 20-24.

[6] H Ajer, S Landrø, and K Stenersen (1994): Numerical simulations of thermal focusing and thermally induced birefringence effects in diode side-pumped solid state lasers, *Proceedings from the Conference on Lasers and Electro-Optics Europe 1994* (CLEO-E 1994), paper CFH2.

[7] T Y Fan (1993): Heat generation in Nd:YAG and Yb:YAG, *IEEE J Quantum Electron*, Vol 29, pp 1457-1459.

[8] D C Brown (1998): Heat, fluorescence, and stimulated-emission power densities and fractions in YAG, *IEEE J Quantum Electron*, Vol 34, pp 560-571.

DISTRIBUTION LIST

FFIE **Dato:** 30 juli 2001

RAPPORTTYPE (KRYSS AV)	RAPPORT NR.	REFERANSE	RAPPORTENS DATO
X RAPP ☐ NOTAT ☐ RR	2001/03865	FFIE/792/115	30 juli 2001
RAPPORTENS BESKYTTELSESGRAD		ANTALL EKS UTSTEDT	ANTALL SIDER
Unclassified		40	33
RAPPORTENS TITTEL		FORFATTER(E)	
THERMAL EFFECTS IN END-PUMPED SOLID STATE LASERS - Influence on resonator stability, beam quality, and output power		STENERSEN Knut, LIPPERT Espen, RUSTAD Gunnar, ARISHOLM Gunnar	
FORDELING GODKJENT AV FORSKNINGSSJEF:		FORDELING GODKJENT AV AVDELINGSSJEF:	

EKSTERN FORDELING

ANTALL	EKS NR	TIL
1		FO/FST
1		FO/FST, v/Oblt Gaute Dyrdal,
1		LTI, EK-kontoret
1		HFK
1		HFK, v/Rittm Tarjei Holtestaul
1		HFK, v/Oing Jan I Smeland
1		LFK
1		LFK, v/Kapt Egil Strømsvåg
1		SFK
1		SFK, v/Orlkapt Bjarne Isfeldt
		www.ffi.no

INTERN FORDELING

ANTALL	EKS NR	TIL
11		FFI-Bibl
1		Adm direktør/stabssjef
1		FFIE
1		FFISYS
1		FFIBM
1		FFIN
1		Halvor Ajer, FFIE
1		Gunnar Arisholm, FFIE
1		Trond Brudevoll, FFIE
1		Harald Hovland, FFIE
1		Espen Lippert, FFIE
1		Stian Løvold, FFIE
1		Gunnar Rustad, FFIE
1		Knut Stenersen, FFIE
1		Gunnar Wang, FFIE
5		Arkiv, FFIE
		FFI-veven

FFI-K1 Retningslinjer for fordeling og forsendelse er gitt i Oraklet, Bind I, Bestemmelser om publikasjoner for Forsvarets forskningsinstitutt, pkt 2 og 5. Benytt ny side om nødvendig.